Supporting Information for

$TiO_2/BiVO_4$ Nanowire Heterostructure Photoanodes based on Type II Band Alignment

Joaquin Resasco[1], Hao Zhang[2], Nikolay Kornienko[2], Nigel Becknell[2], Hyunbok Lee[3] Jinghua Guo[4], Alejandro L. Briseno[5], and Peidong Yang[2,6,7]*

1.Department of Chemical Engineering, and 2.Department of Chemistry, University of California, Berkeley, California 94720, United States. [3.] Department of Physics, Kangwon National University, Chuncheon-si, Gangwon-do 200-701, South Korea. 4. Advanced Light Source Lawrence Berkeley National Laboratory, Berkeley, California 94720, United States. 5.Department of Polymer Science & Engineering, Conte Polymer Research Center, University of Massachusetts, Amherst, Massachusetts 01003,United States. 6.Materials Sciences Division, and 7. Kavli Energy NanoSciences Institute, Lawrence Berkeley National Laboratory, Berkeley, California 94720, United States.

Table of contents:

Supplementary Figures

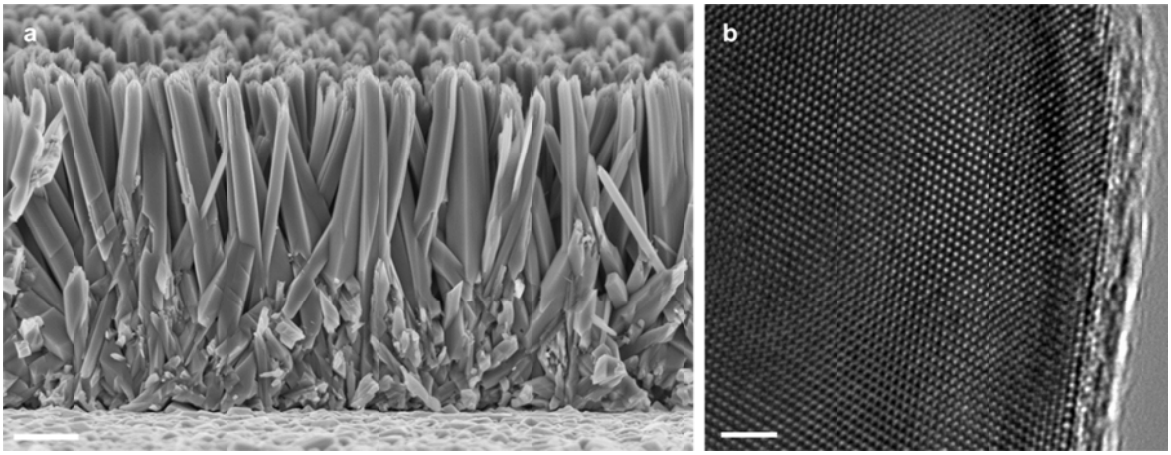

Figure S1: (a) Cross-sectional SEM of TiO_2 nanowires (b) HRTEM of TiO_2 nanowires consistent with a single crystal rutile TiO_2 structure and c-axis growth direction.

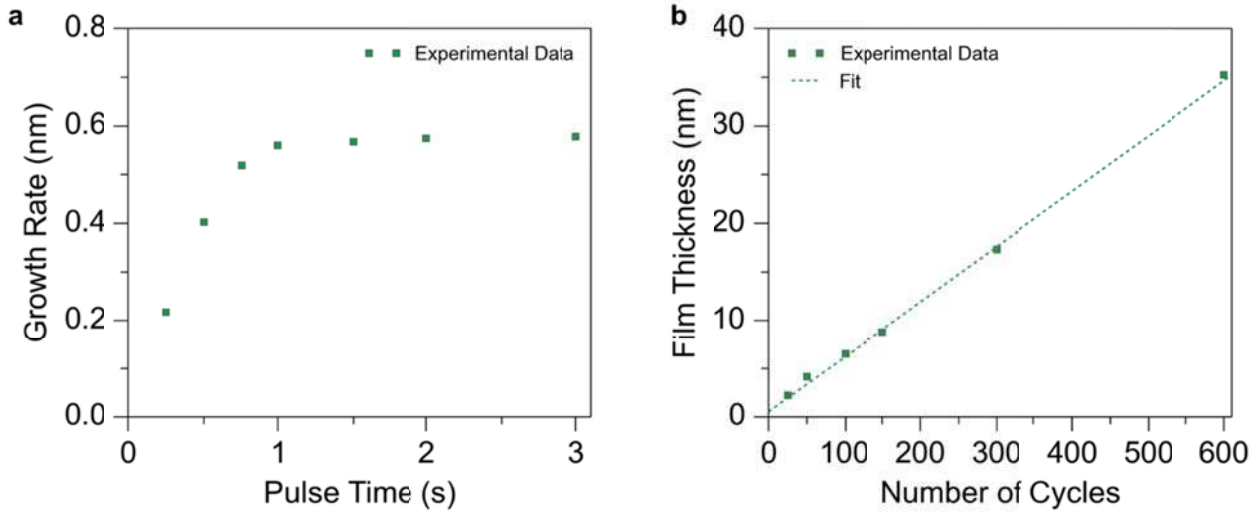

Figure S2: (a) Growth rate per cycle of Ta_2O_5 ALD films under increasing pulse time of the Ta precursor. Saturation was observed after 1.0 s. (b) Thickness of Ta_2O_5 ALD films measured by ellipsometry as a function of number of cycles. A linear growth rate of ~0.6 Å/cycle was observed.

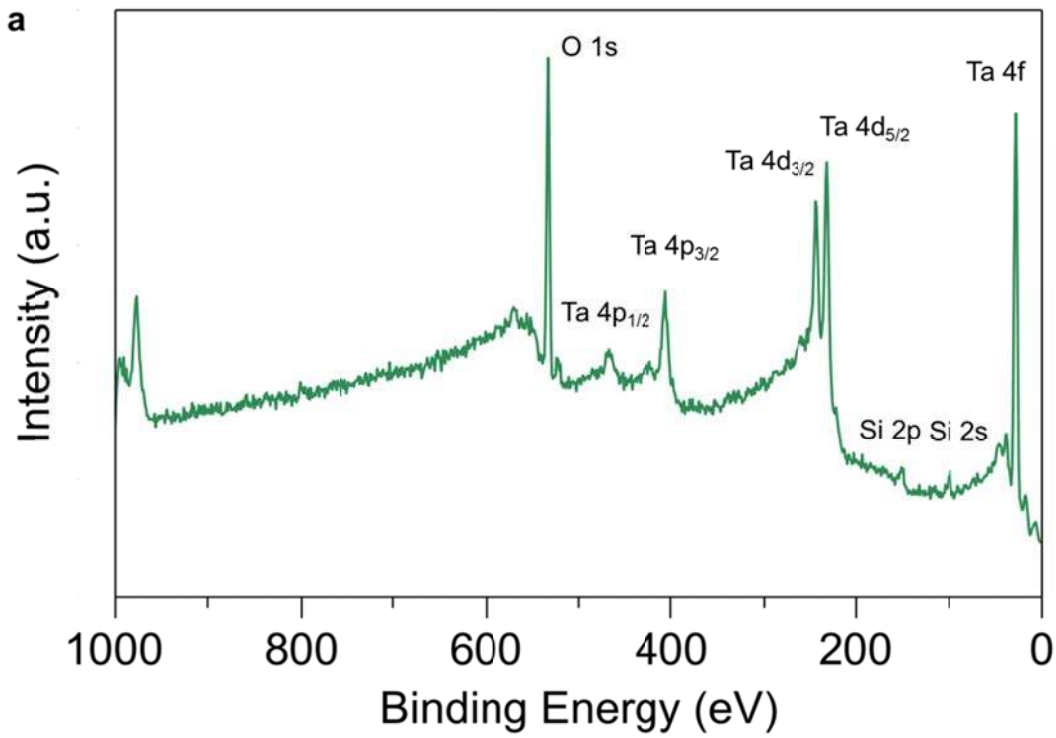

Figure S3: (a) X-ray photoelectron spectrum of Ta_2O_5 ALD thin film deposited on a Si wafer following a 1 min Ar sputter. The lack of organic contamination signifies complete substitution of ligands by oxygen from the H_2O precursor pulse.

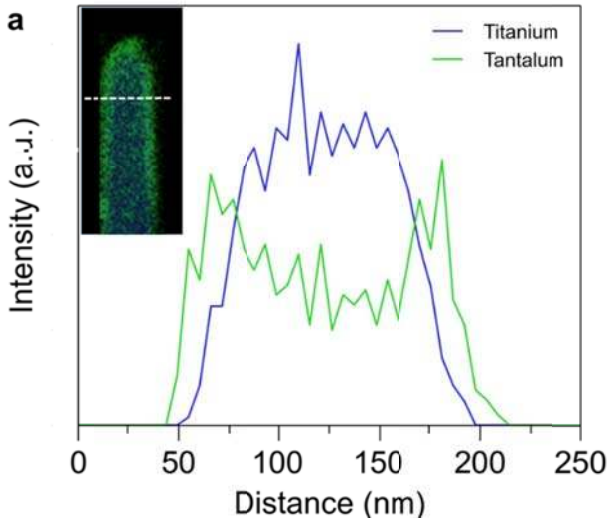

Figure S4: (a) Line scan of $TiO_2|Ta_2O_5$ core-shell nanowire showing a uniform Ta_2O_5 film coating the high surface area nanowires.

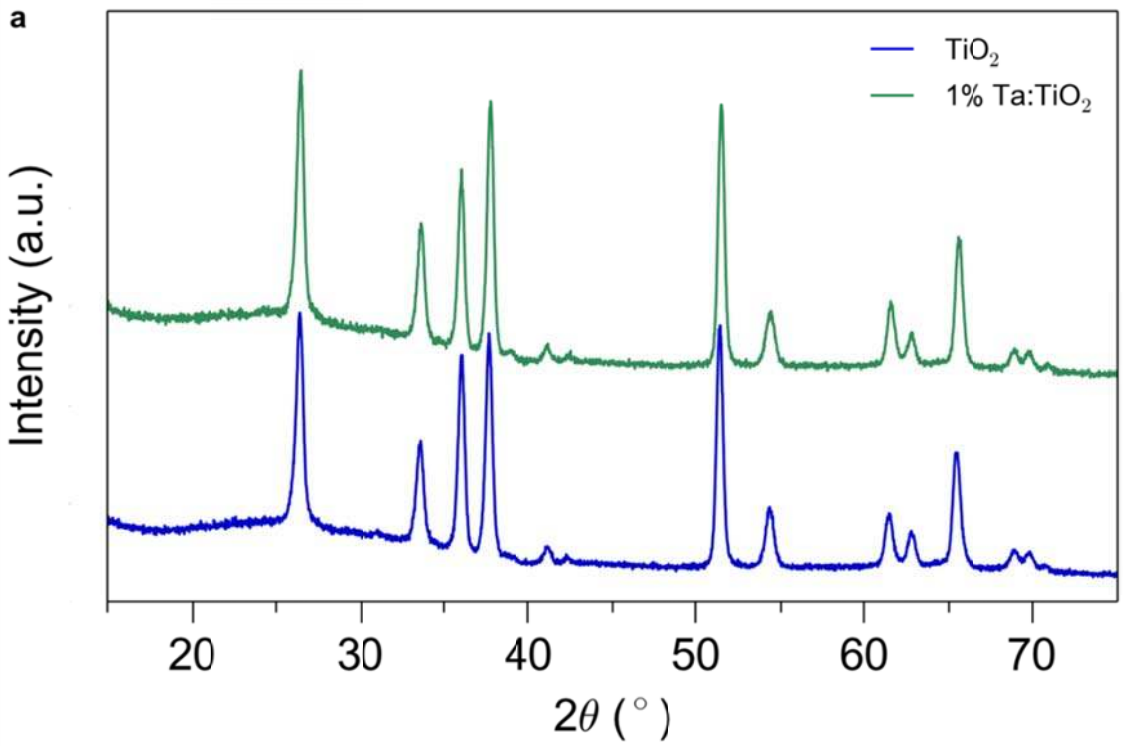

Figure S5: (a) X-Ray Diffraction patterns of TiO_2 nanowire samples before and after incorporation of Ta dopants. The crystal structure of the nanowires is unchanged by the doping process.

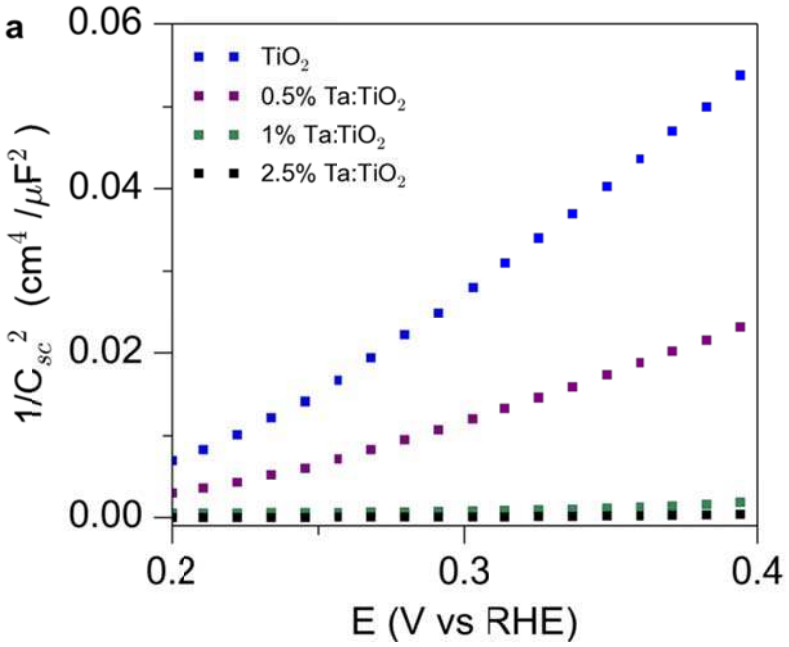

Figure S6: Mott-Schottky plots of various levels of Ta doping showing an increase in carrier concentration with increased concentration of Ta.

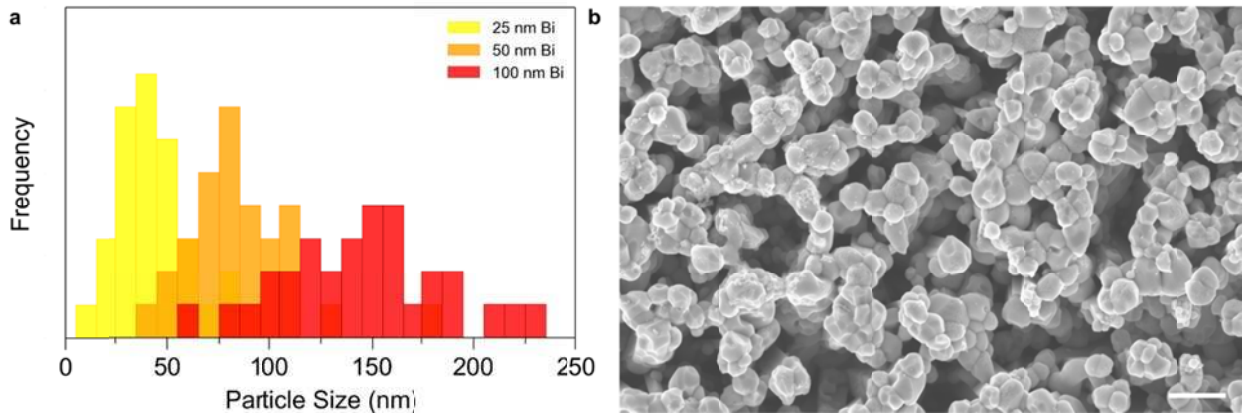

Figure S7: (a,b) Particle size statistics and representative SEM image of Ta:TiO_2|$BiVO_4$ sample with 100 nm Bi planar equivalent loading. Average particle sizes for 25, 50, and 100 nm planar equivalents are 45 nm, 85 nm, and 148 nm, respectively. Scale bar is 500 nm.

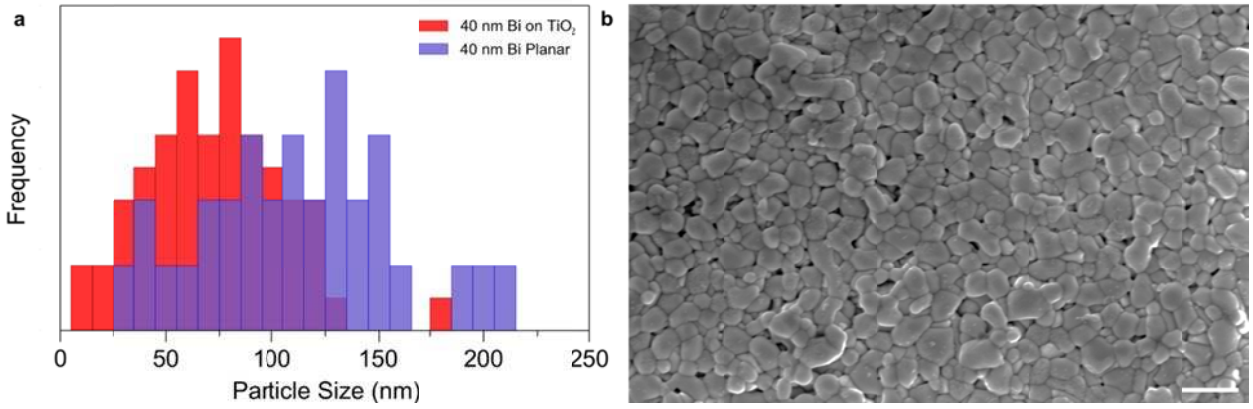

Figure S8: (a) Particle size statistics for planar vs nanowire loaded $BiVO_4$. The nanowire array prevents large particle growth. (b) Representative SEM image of a planar $BiVO_4$ sample with 40 nm Bi planar equivalent loading. Average particle sizes for nanowire and planar samples are 72 nm and 117 nm, respectively. Scale bar is 500 nm.

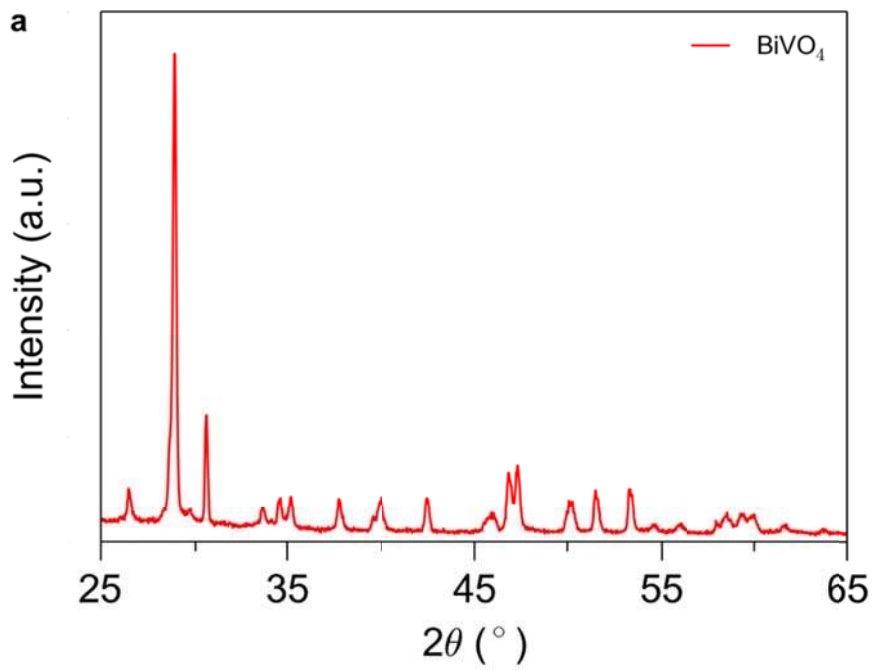

Figure S9: (a) X-Ray Diffraction patterns of planar $BiVO_4$, showing the diffraction pattern of the monoclinic scheelite $BiVO_4$ phase.

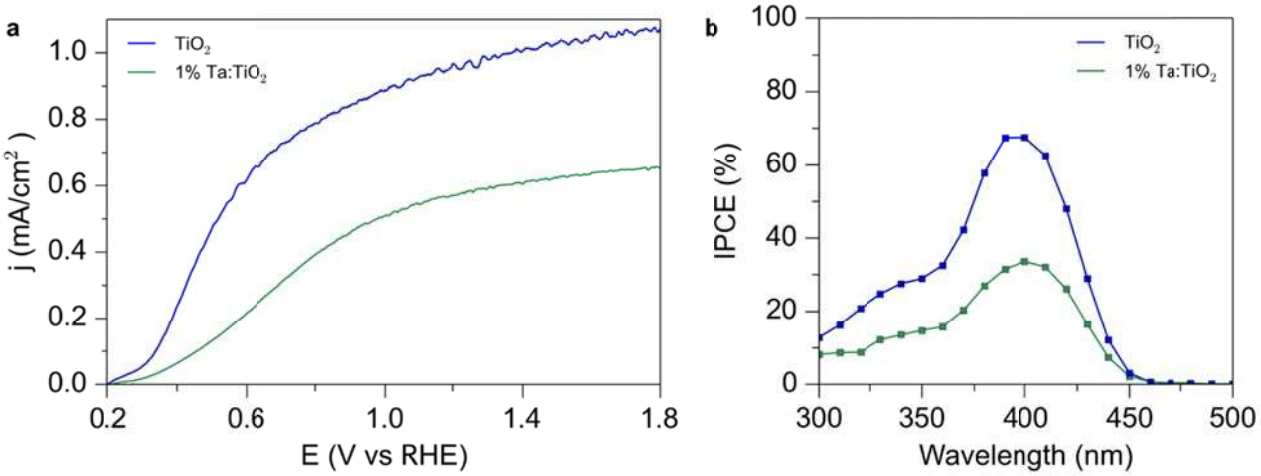

Figure S10: (a) Linear sweep voltammograms of TiO_2 and Ta:TiO_2 nanowire samples. Decreased activity for water oxidation is observed after Ta doping. (b) IPCE data for TiO_2 and Ta:TiO_2 nanowire samples.

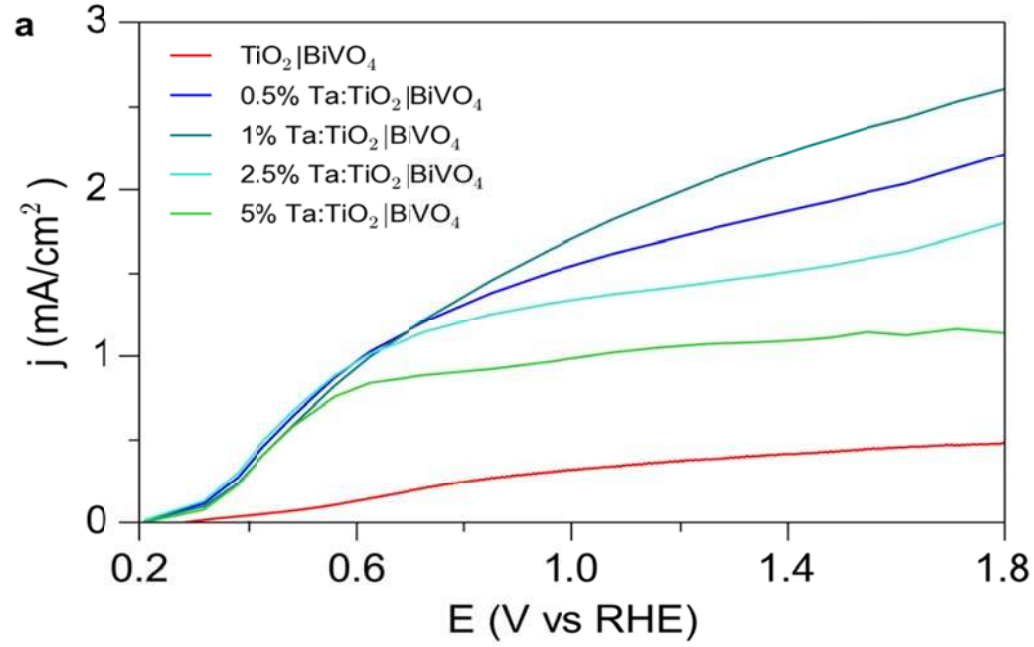

Figure S11: (a) Linear sweep voltammograms of TiO_2 and Ta:TiO_2 nanowire samples loaded with 40 nm $BiVO_4$. An optimum in performance is observed for 1% Ta doping.

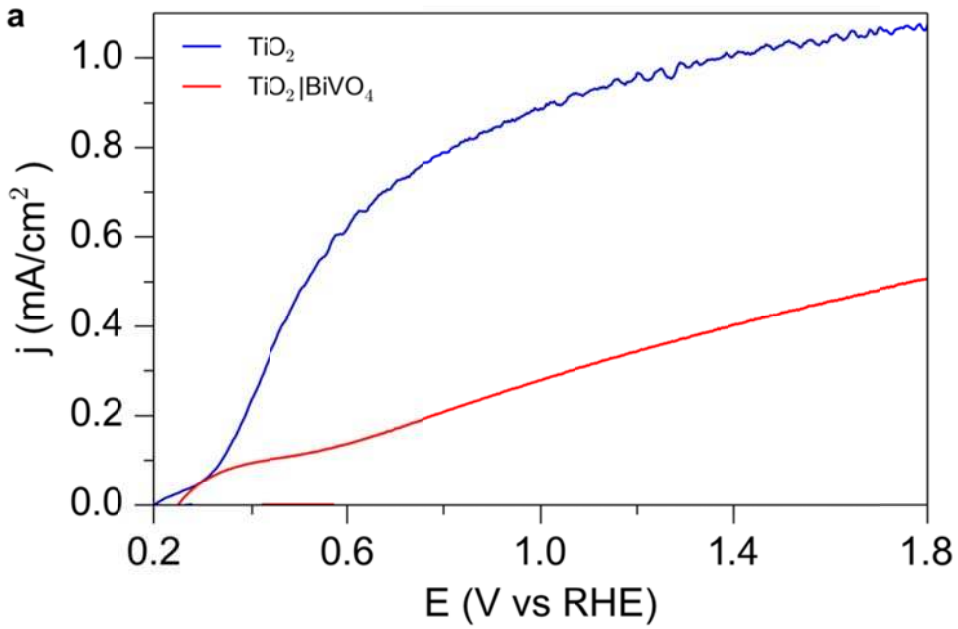

Figure S12: (a) Linear sweep voltammograms of TiO_2 and TiO_2|$BiVO_4$ samples. Decreased activity for water oxidation is observed after addition of $BiVO_4$, possibly due to poor electron transport between TiO_2 and $BiVO_4$.

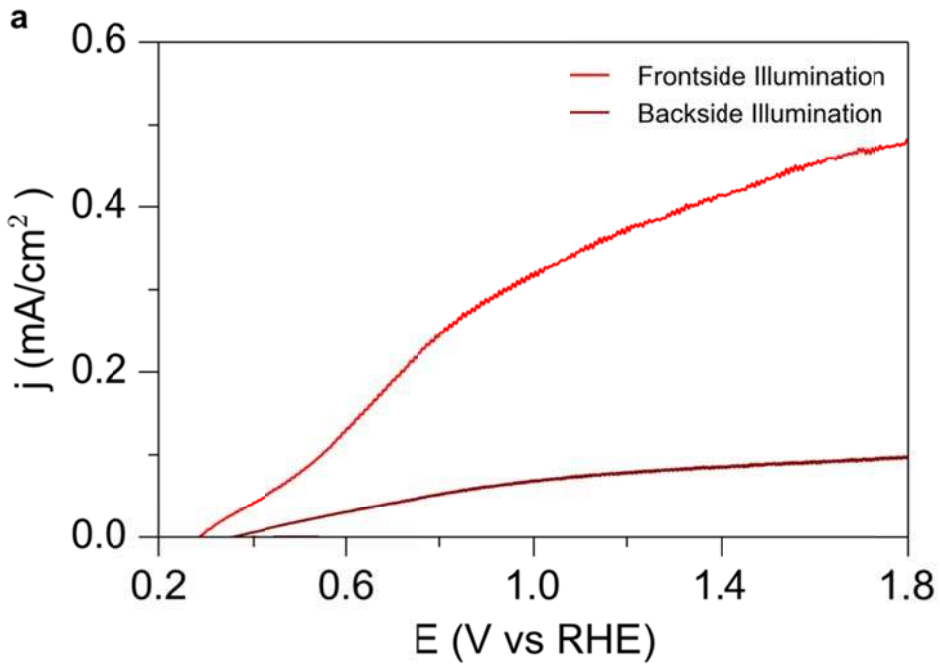

Figure S13: (a) Linear sweep voltammograms of TiO_2|$BiVO_4$ samples under frontside and backside illumination. Electron transfer from TiO_2 to $BiVO_4$ would result in higher backside photocurrent as carriers generated in TiO_2 near the back electrode would be collected. Instead, the frontside current is much higher, indicating electron transfer is from $BiVO_4$ to TiO_2.

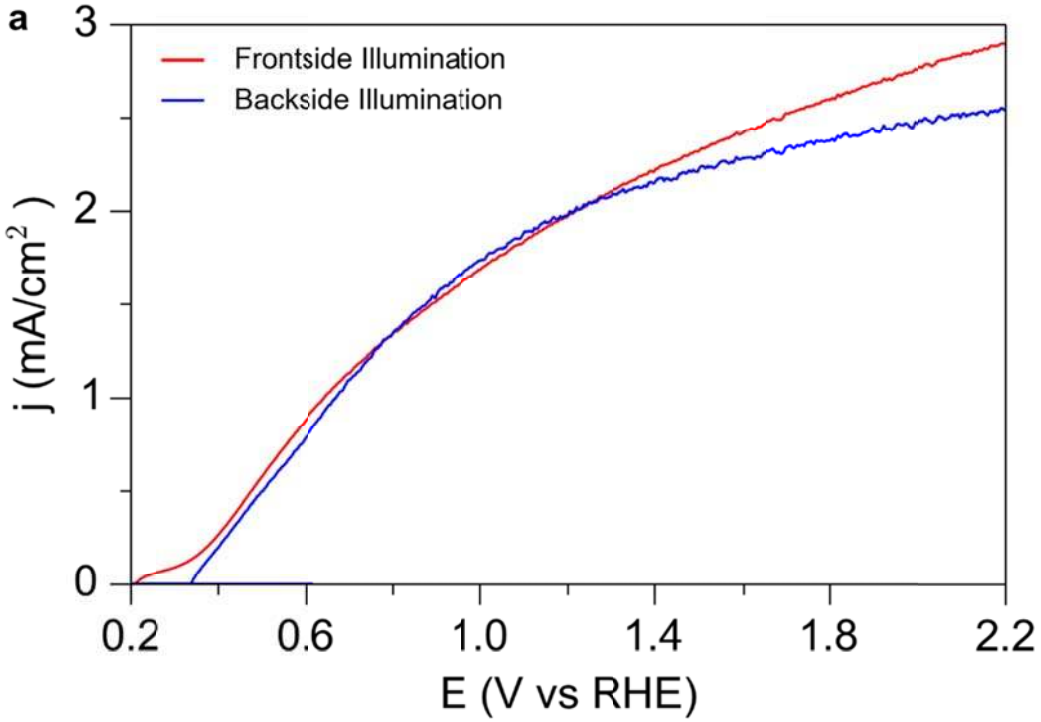

Figure S14: Linear sweep voltammograms of 1% Ta:TiO_2|$BiVO_4$ samples under frontside and backside illumination. At optimal loading, performance is similar under frontside and backside illumination.

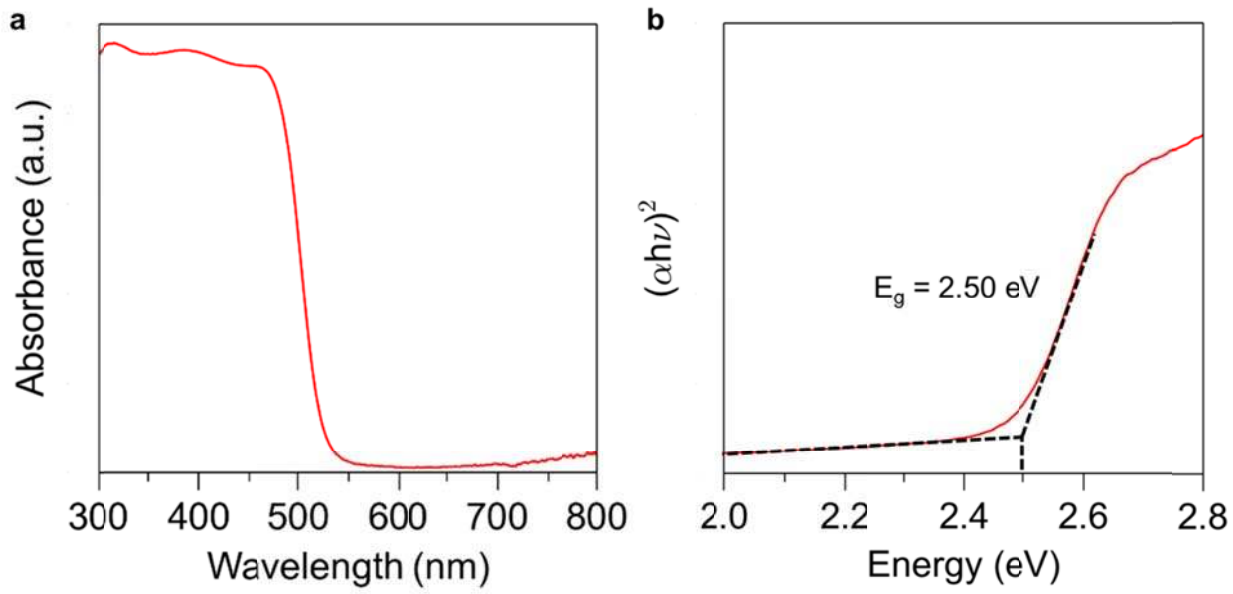

Figure S15: (a) Optical absorption and (b) Tauc plot of a $BiVO_4$ thin film deposited on FTO/glass assuming the optical band gap of $BiVO_4$ is a direct transition.

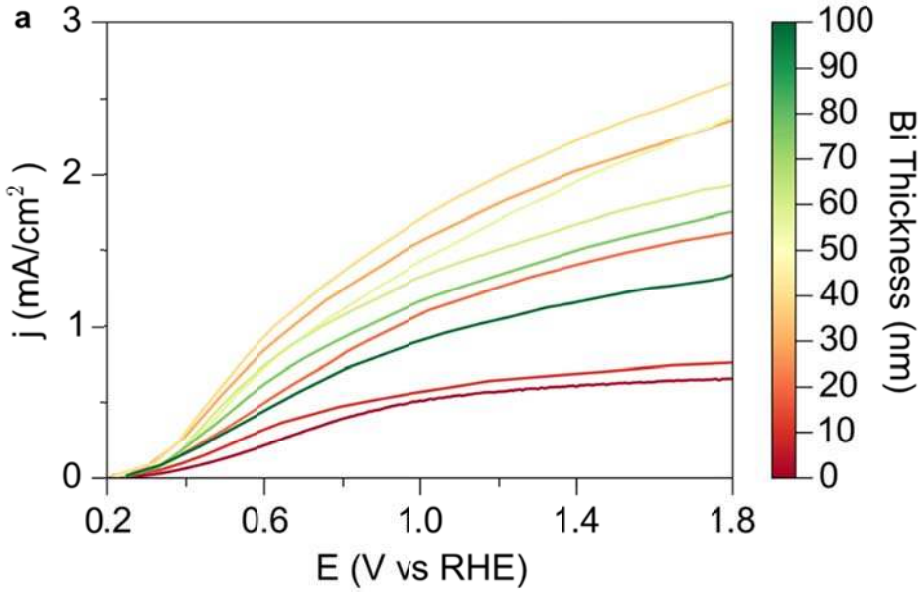

Figure S16: Linear sweep voltammograms of different loadings of $BiVO_4$ on 1% Ta:TiO_2. An optimum is observed for 40 nm Bi.

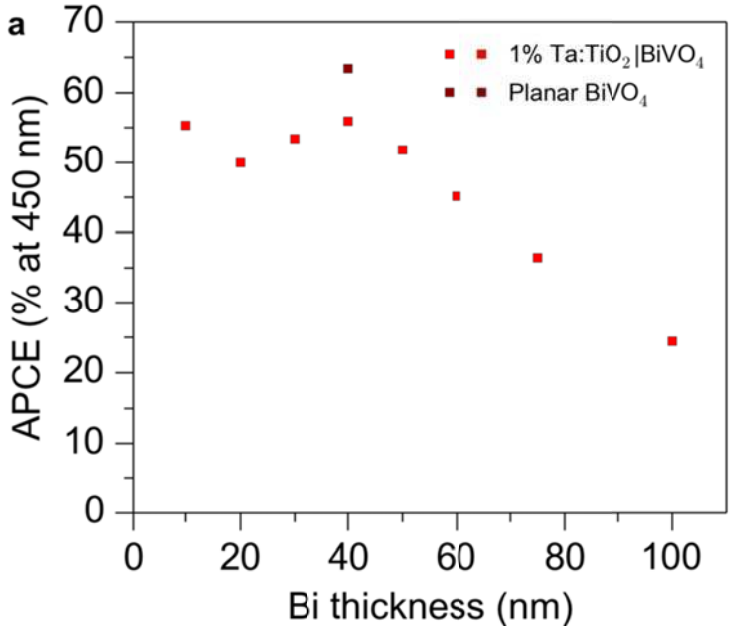

Figure S17: (a) APCE for Ta:TiO_2|$BiVO_4$ samples with increasing loading. High APCE values are observed for planar equivalent thickness <60 nm. Planar $BiVO_4$ shows higher APCE than Ta:TiO_2|$BiVO_4$ at equal loading but is limited by insufficient absorption.

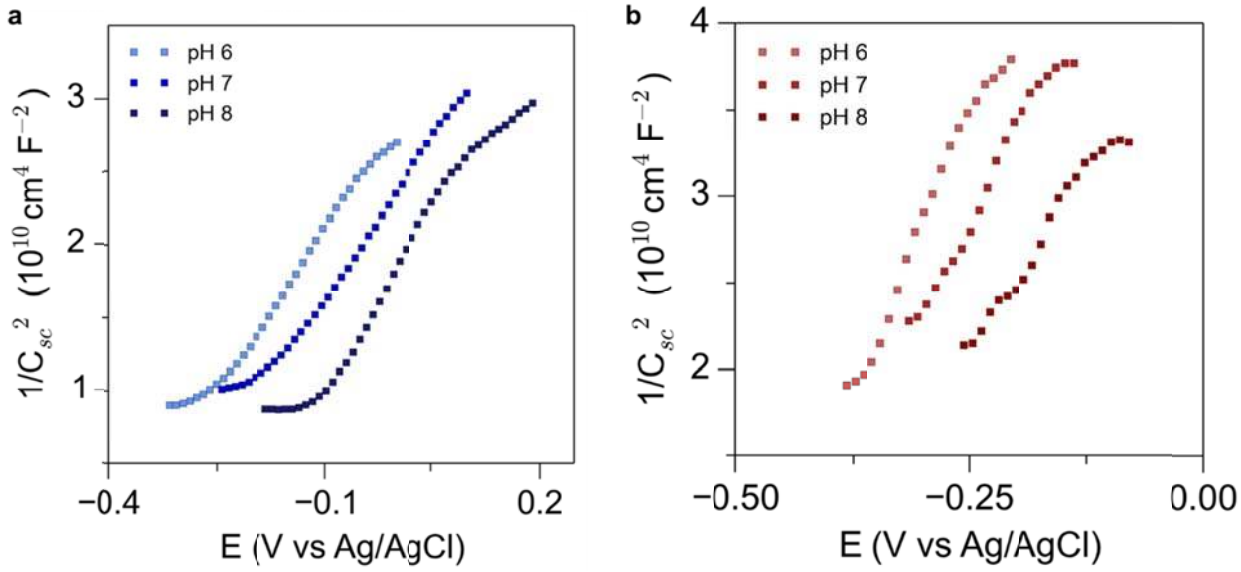

Figure S18: (a,b) Mott-Schottky plots for TiO_2 and $BiVO_4$. E_{fb} is observed to shift ~59 mV/pH.

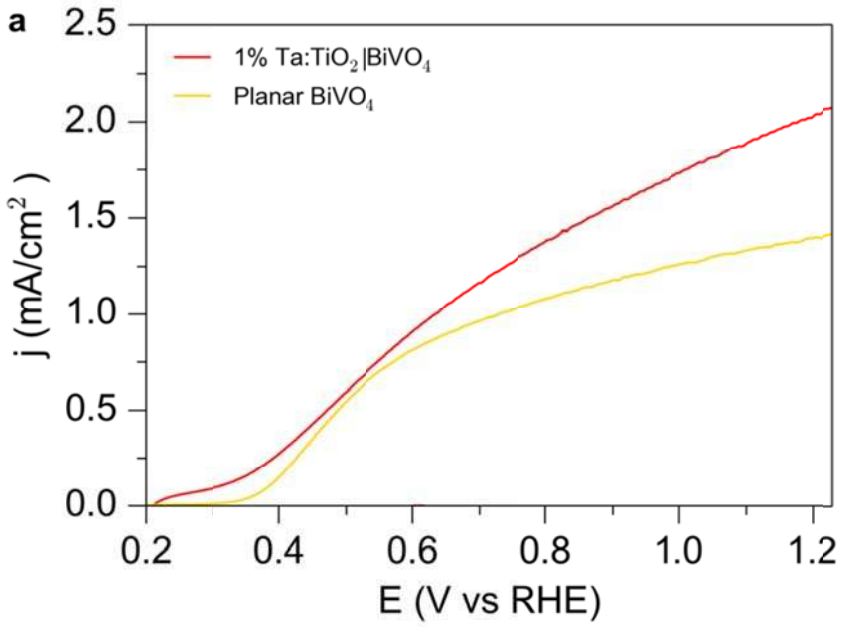

Figure S19: (a) Linear sweep voltammograms of Ta:TiO_2|$BiVO_4$ and planar $BiVO_4$ samples. Lower activity for water oxidation is observed for the unsupported samples due to incomplete light absorption.

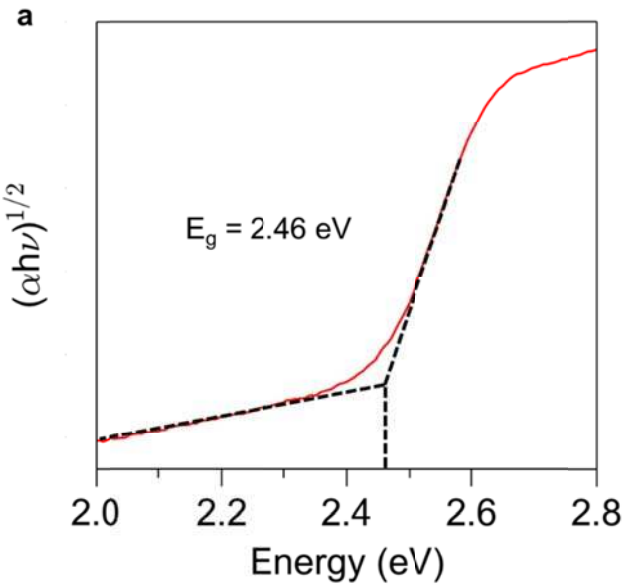

Figure S20: (a) Tauc plot of a $BiVO_4$ thin film deposited on FTO/glass assuming the optical band gap of $BiVO_4$ is an indirect transition. A smaller band gap is observed consistent with the work of Cooper et al.[1]

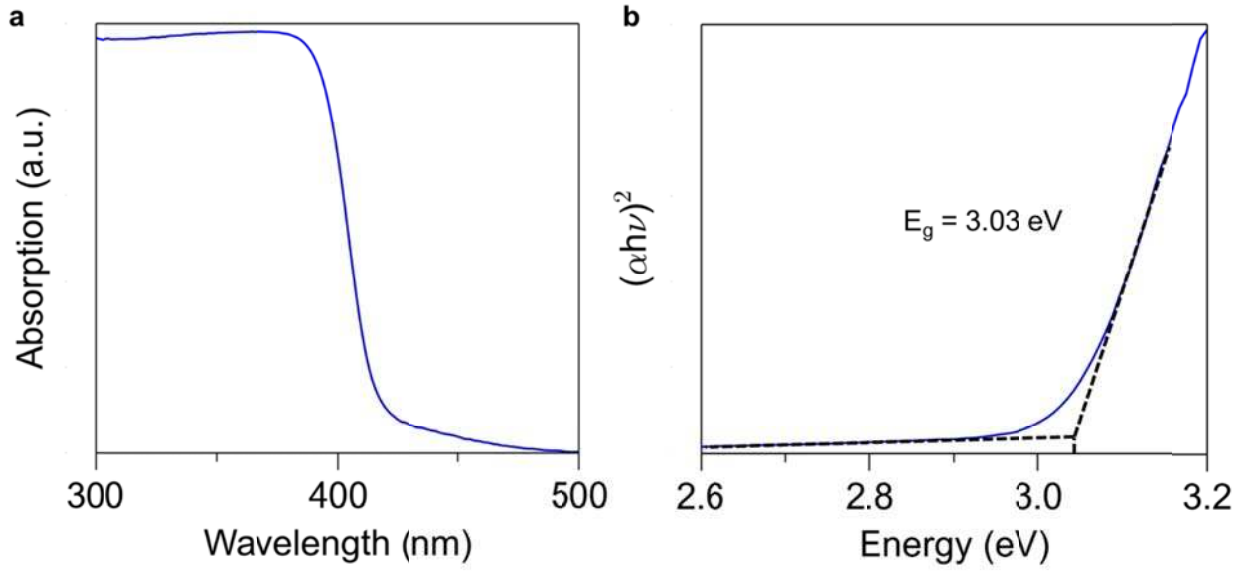

Figure S21: (a) Optical absorption and (b) Tauc plot of TiO_2 nanowire samples on FTO/glass assuming the optical band gap of TiO_2 is a direct transition.

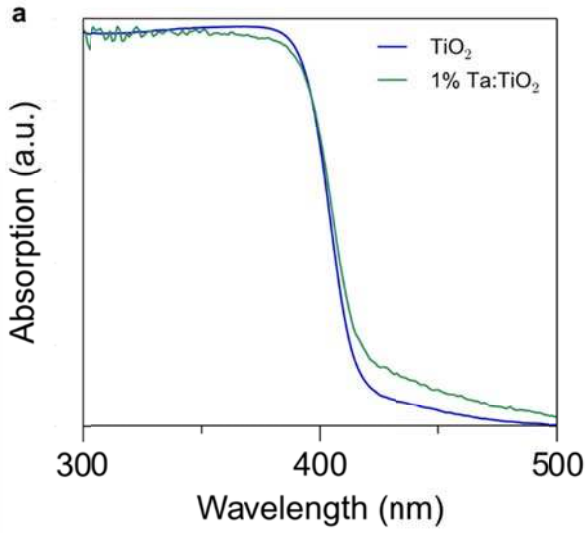

Figure S22: (a) Optical absorption of TiO_2 and Ta:TiO_2 nanowire samples demonstrating the optical absorption is not significantly changed by the doping process.

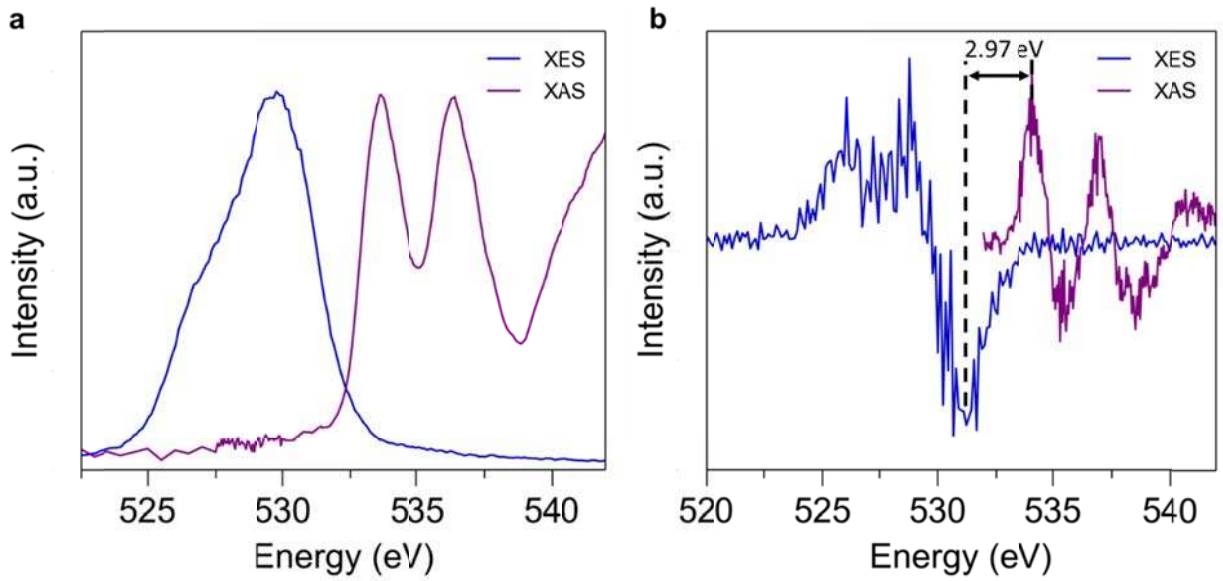

Figure S23: (a) Combined X ray absorption and emission spectra for TiO_2. (b) Derivative spectrum of (a). The difference between the local maximum of the XAS spectrum and local minimum of the XES spectrum gives the electronic band gap.

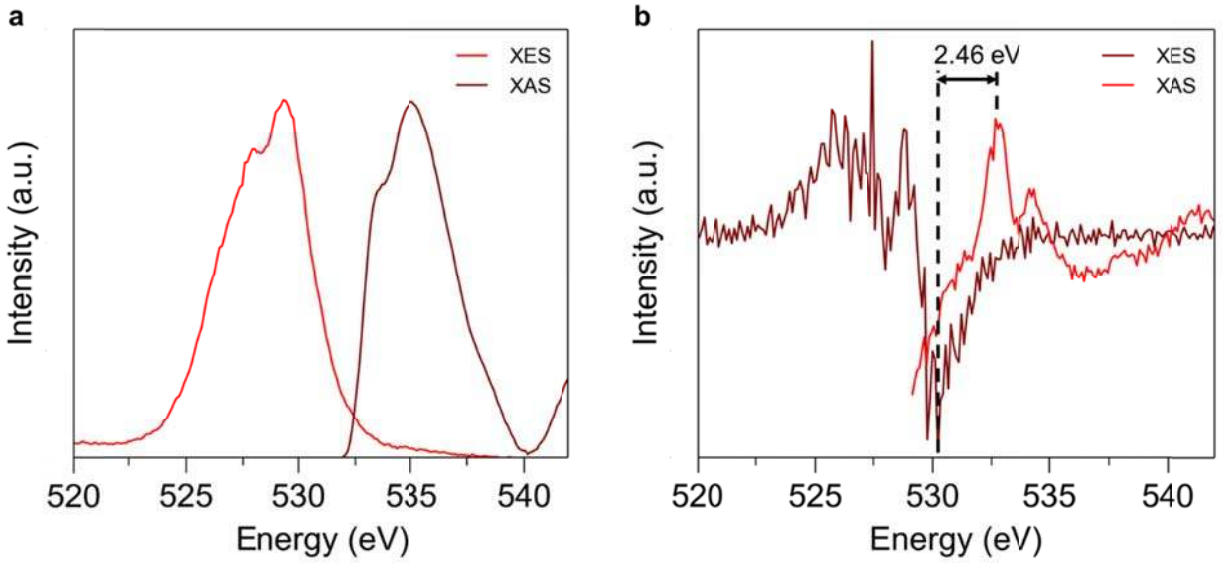

Figure S24: (a) Combined X ray absorption and emission spectra for $BiVO_4$. (b) Derivative spectrum of (a). The difference between the local maximum of the XAS spectrum and local minimum of the XES spectrum gives the electronic band gap.

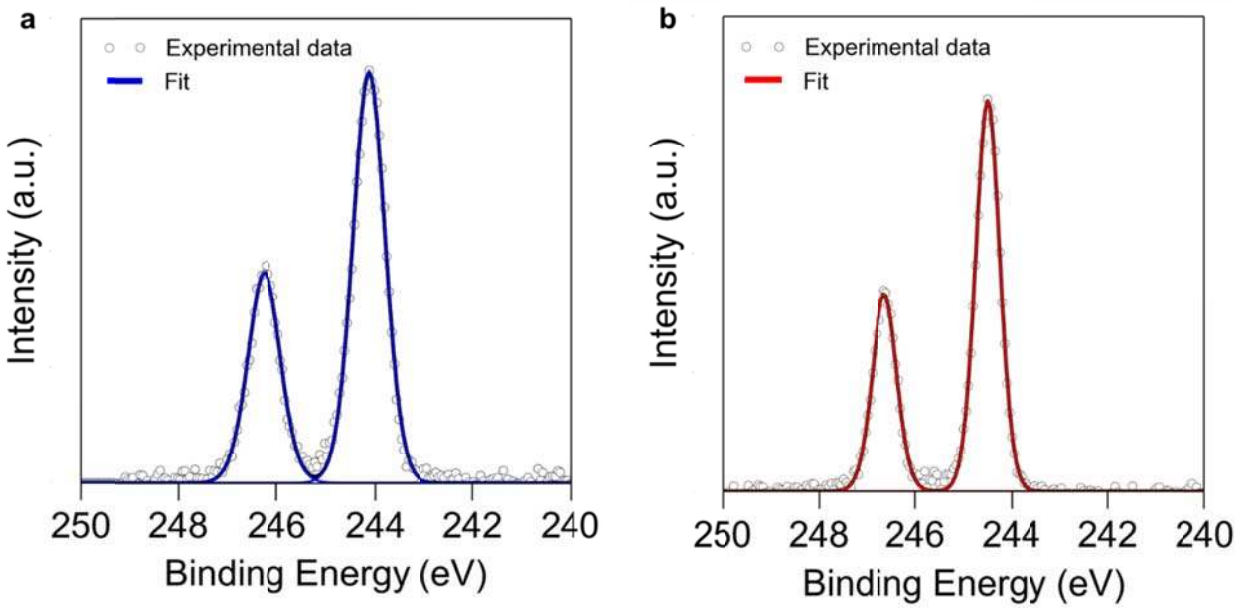

Figure S25: (a,b) Ar 2p XPS spectra taken in the near surface region of TiO_2 and $BiVO_4$. The work function is related to the Ar $2p_{3/2}$ binding energy values. The work function of TiO_2 is estimated to be ~0.2 eV larger than that of $BiVO_4$.

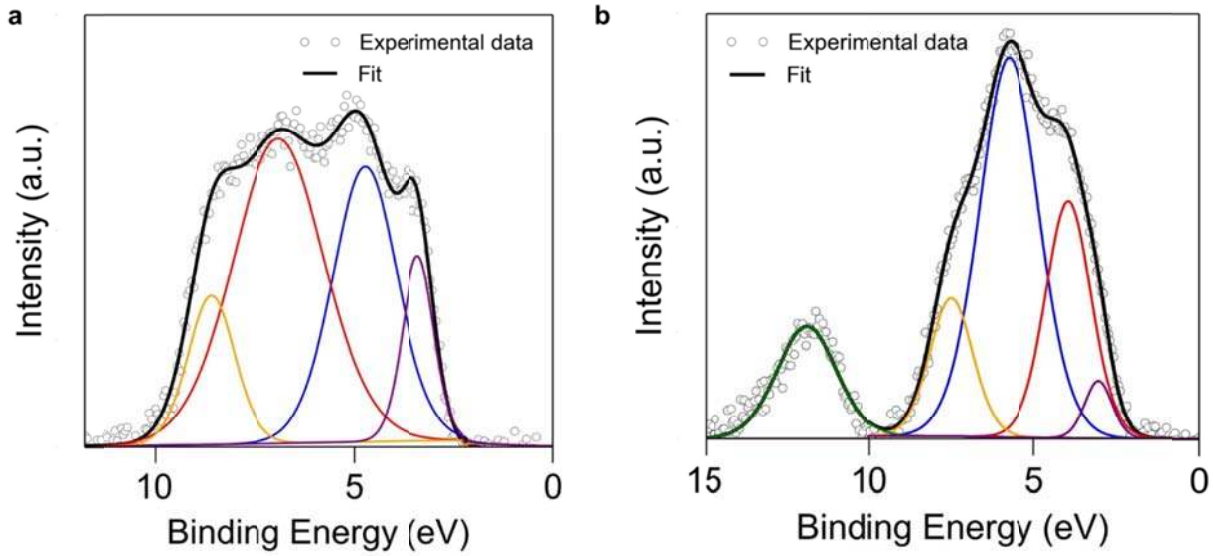

Figure S26: (a,b) Valence band electronic structure of TiO_2 and $BiVO_4$ measured using XPS.

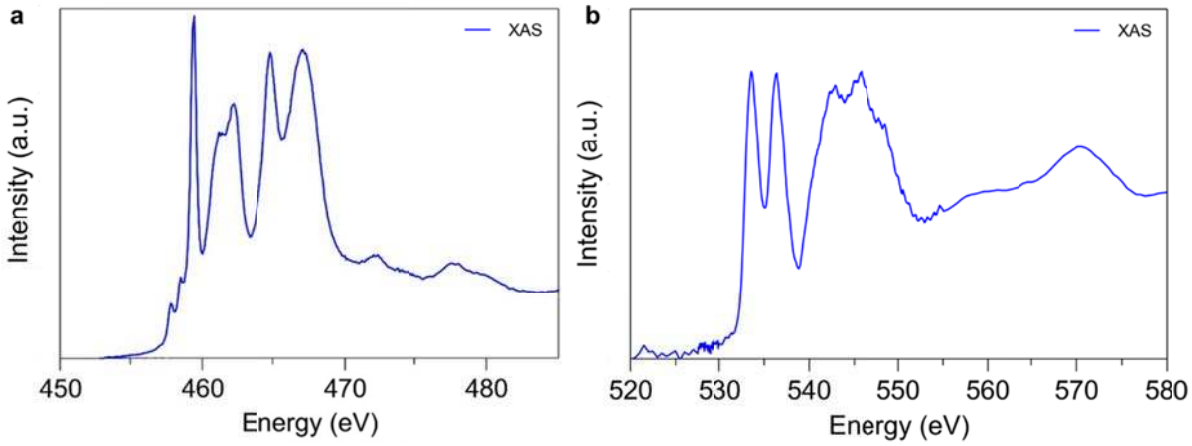

Figure S27: (a,b) Ti L edge and O K edge X-ray absorption spectra for TiO_2. Total electron yield (TEY) data is shown, as no significant differences were observed between TEY and fluorescence yield data.

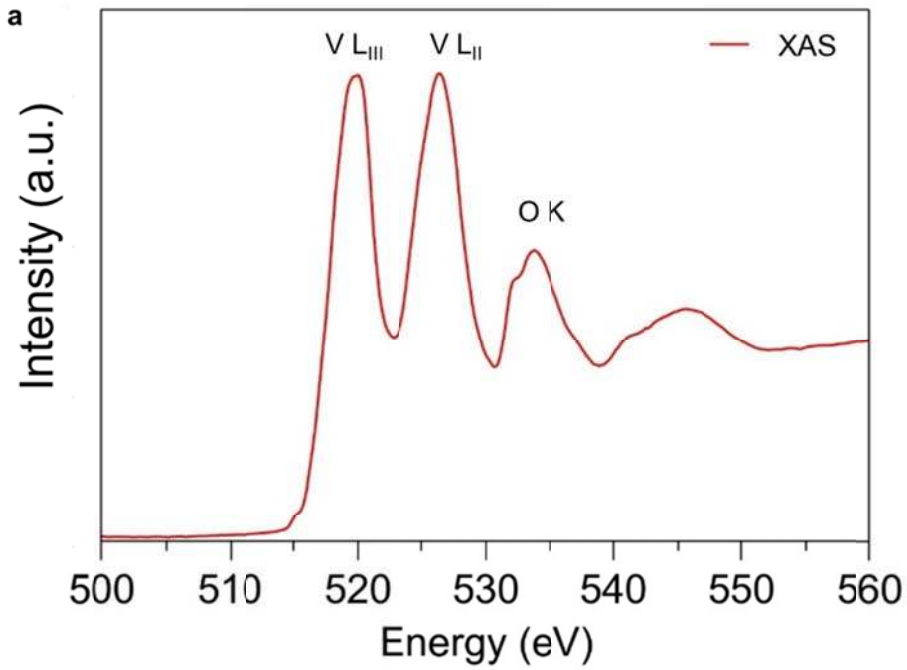

Figure S28: (a) V L edge and O K edge X-ray absorption spectra for $BiVO_4$. Total electron yield (TEY) data is shown, as no significant differences were observed between TEY and fluorescence yield data.

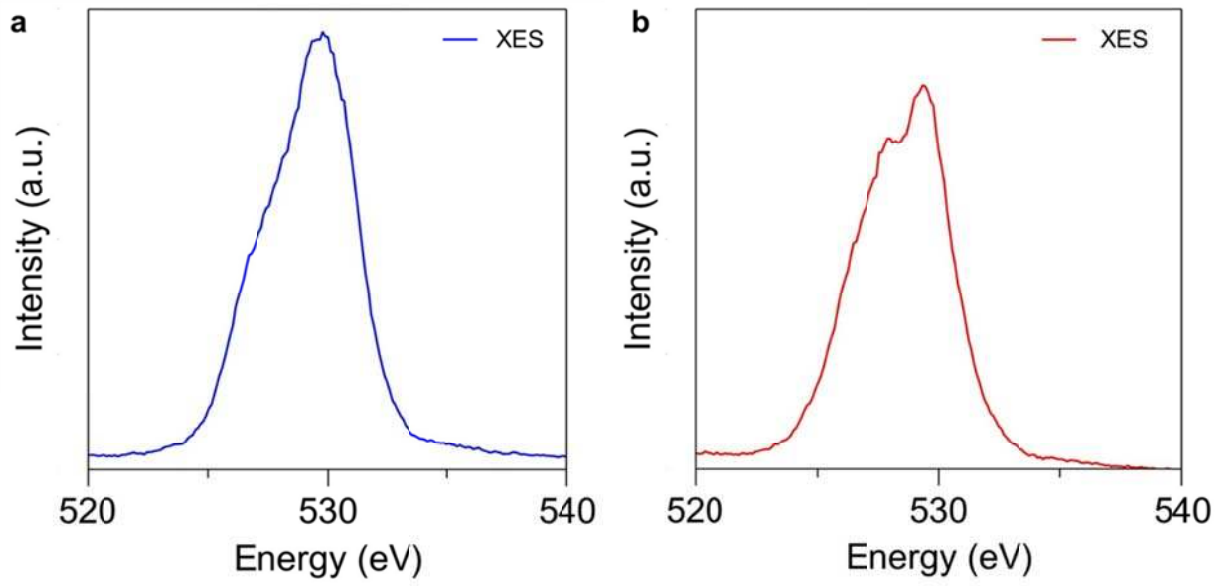

Figure S29: (a,b) X ray emission spectra of TiO_2 and $BiVO_4$ measured at an excitation energy of 590 eV.

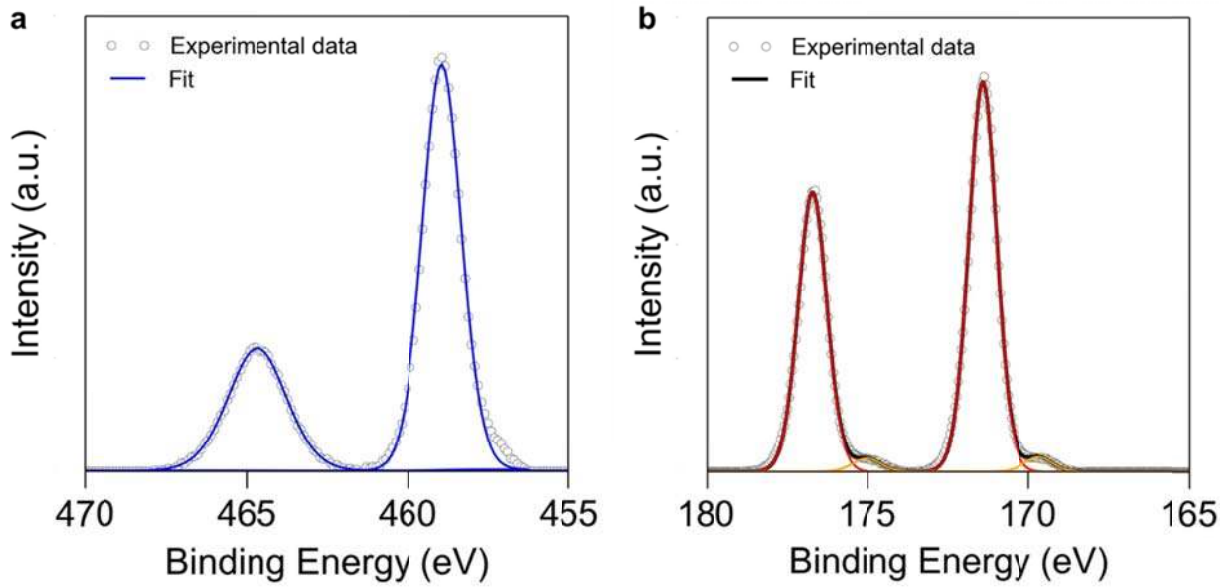

Figure S30: (a,b) XPS spectra of the Ti 2p level for TiO_2 and Bi 4f level for $BiVO_4$.

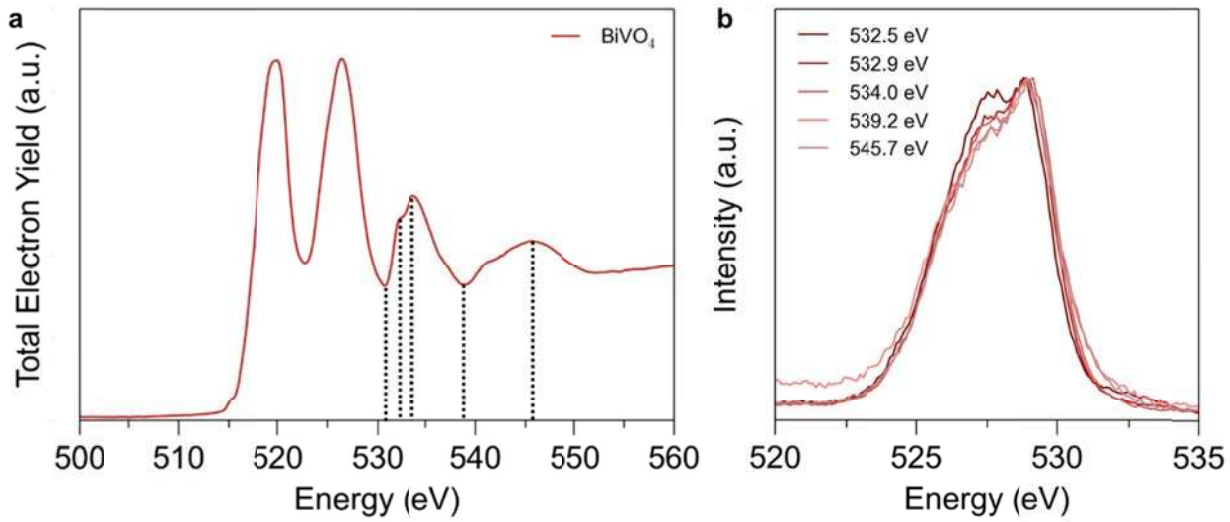

Figure S31: (b) RIXS spectra for $BiVO_4$ on the O K edge. Excitation energies are specified on the XAS spectrum in (a).

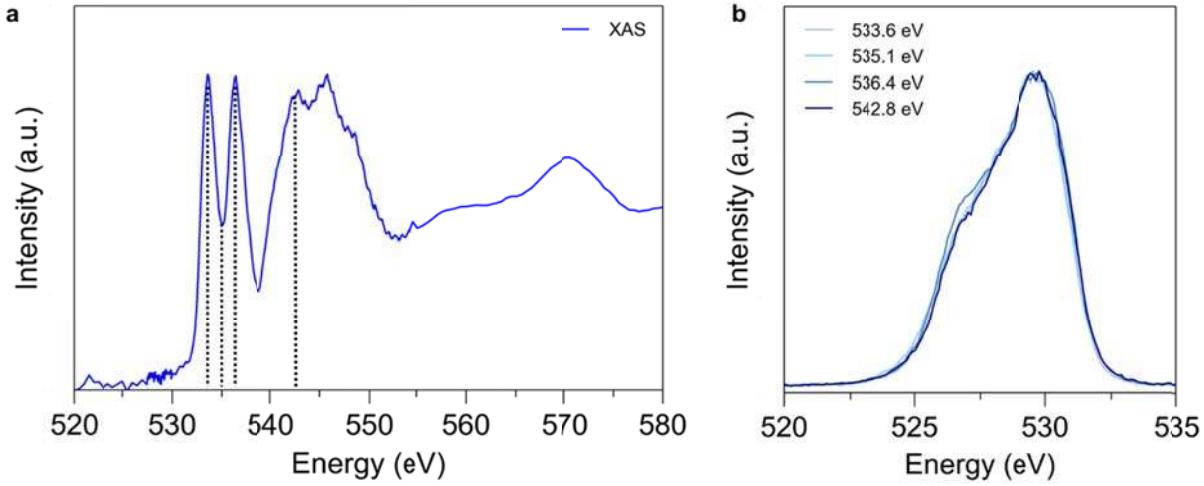

Figure S32: (b) RIXS spectra for TiO_2 on the O K edge. Excitation energies are specified on the XAS spectrum in (a).

Supplementary References:

1. Cooper, J. K.; Gul, S.; Toma, F. M.; Chen, L.; Liu, Y.-S.; Guo, J.; Ager, J. W.; Yano, J.; Sharp, I. D. *The Journal of Physical Chemistry C* **2015,** 119, (6), 2969-2974.